OPEN

PIN architecture for ultrasensitive organic thin film photoconductors

Zhiwen Jin & Jizheng Wang

Beijing National Laboratory for Molecular Sciences, CAS Key Laboratory of Organic Solids, Institute of Chemistry, Chinese Academy of Sciences, Beijing 100190, China.

Organic thin film photoconductors (OTFPs) are expected to have wide applications in the field of optical communications, artificial vision and biomedical sensing due to their great advantages of high flexibility and low-cost large-area fabrication. However, their performances are not satisfactory at present: the value of responsivity (R), the parameter that measures the sensitivity of a photoconductor to light, is below 1 AW^{-1}. We believe such poor performance is resulted from an intrinsic self-limited effect of present bare blend based device structure. Here we designed a PIN architecture for OTFPs, the PIN device exhibits a significantly improved high R value of 96.5 AW^{-1}. The PIN architecture and the performance the PIN device shows here should represent an important step in the development of OTFPs.

Photoconductors have great applications in the field of optical communications, artificial vision and biomedical sensing[1-3]. In recent years, inexpensive, ultrathin and stretchable photoconductors are highly demanded in order to meet the rapidly growing requirements in real applications[4-6]. For this purpose, organic π-conjugated small molecules and polymers are selected as excellent material candidates for such photoconductor devices[7]. However, exciton binding energies in organic materials are quite high (0.3 to 1 eV) due to their low dielectric constants (2 to 4), hence photogenerated excitons usually cannot be dissociated into free charge carriers by the thermal energy at room temperature[7,8], and a donor/acceptor interface is usually needed to separate the tightly binded electron-hole pairs. Thereby donor:acceptor blend films are commonly used in organic photoelectric devices as active layers to ensure that enough free photo carriers can be generated[9-11].

Poly(3-hexylthiophene) (P3HT)/6,6-phenyl-C61-butyric acid ethyl ester (PCBM) has been widely used as a classic donor/acceptor combination (P3HT is P-type semiconductor and PCBM is N-type semiconductor), and serves as a solid base for fundamental studies and conceptual demonstrations in organic photoelectric devices[12-15]. For the development of organic thin film photoconductors (OTFPs), in the early days Peet et al.[13] tried to enhance the performance by optimizing the nano-morphology of the P3HT:PCBM blend film to maximize the number of free photo carriers. Later, Liao et al.[14] used [70]PCBM (analogue of PCBM and displays improved light absorption[16]) to replace the PCBM in the blend, the device performance is improved due to the enhanced light absorption. Recently, Li et al.[15] successfully further improved the performance of the P3HT:PCBM photoconductor using a substrate with patterned photonic crystals (which increases the reflection light and hence increases the light absorption of the blend film). However, performances of these devices remain unsatisfactory: responsivity (R), the parameter characterizing the sensitivity of a photoconductor to light, is below 1 AW^{-1}. Realizing high-performance OTFPs still remains a big challenge today.

Organic materials show innate nature of high absorption coefficients (exceeding 10^5 cm^{-1})[7], which is a big advantage for them to serve as active layers in photoconductor devices. In present OTFPs, a donor:acceptor blend layer is responsible not only for carrier generation but also for carrier transport. The blend layer is of course good enough for carrier generation, but not for carrier transport: carrier mobilities in a blend layer are usually very low because carriers have to travel a long way inside the nanoscale network of the blend[17]. Thereby we believe that performances of present OTFPs are self-limited by the bare blend based device structure. Additional layers with high carrier mobilities should be brought in to replace the low-mobility blend layer to transport the photo carriers. Theoretically, an ideal structure for OTFPs should been the PIN architecture which has been widely used in solar cells and photodiode[18,19]. In this paper, we designed a PIN architecture for OTFPs: P3HT/P3HT:PCBM/PCBM. In such a PIN device, the P3HT:PCBM blend layer (I-layer), the P3HT layer (P-layer) and the PCBM layer (N-layer) are responsible for carrier generation, hole transport and electron transport, respectively. Since electron (hole) mobility in the PCBM (P3HT) film is much higher than that in the P3HT:PCBM blend film, the PIN photoconductor exhibits excellent performance, R as high as 96.5 AW^{-1} is achieved (more than 100-fold improvement
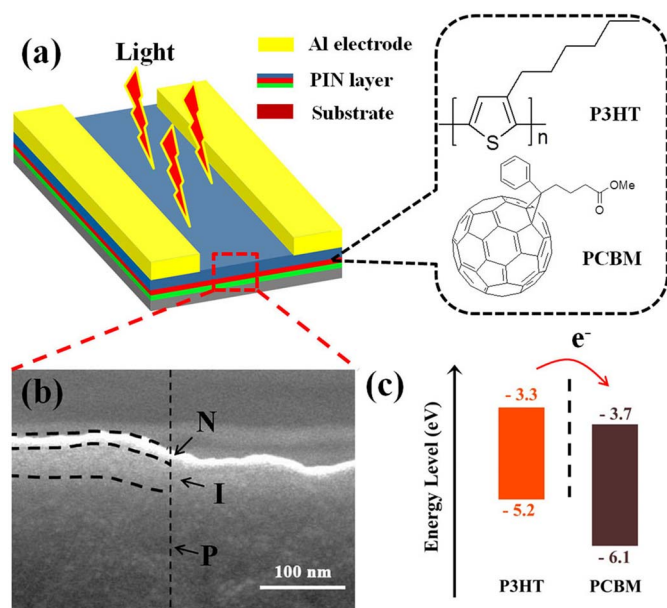
Figure 1 | (a) Schematic illustration of the PIN photoconductor and the molecular structures of P3HT and PCBM. (b) The cross-sectional SEM image of the fabricated PIN layer. (c) Energy band diagram of P3HT and PCBM.

over that of present reported OTFPs). D* (normalized detectivity), G (photoconductive gain) and LDR (linear dynamic range) of the PIN device are 5.69×10^{14} Jones, 200 and 90 dB, respectively. To our knowledge, these values are all the highest records for OTFPs reported so far.

The fabrication process of the PIN photoconductor is shown in Figure S1: a thick P3HT layer (~500 nm) was firstly spin-coated on a glass substrate, and is regarded as P-layer (P3HT usually exhibits high crystallinity and high hole mobility after solvent annealing[20]). Then a PCBM layer (20 nm) was thermally deposited onto the P3HT film, a bilayer PN (P3HT/PCBM) structure is thus formed. During a soft solvent annealing process (put the bilayer P3HT/PCBM PN film into a closed vessel full of dichloromethane (DCM) stream for 60 s),

the PCBM layer will absorb the DCM vapor and slowly diffuse into the P3HT layer, forming a P3HT:PCBM blend layer, which is regarded as the I-layer. Owing to the high solubility of PCBM in DCM and poor solubility of P3HT in DCM[21,22], only about 40 nm I-layer (the thickness was measured by X-ray photoelectron spectroscopy (XPS)) is formed on top of the thick P-layer (~500 nm). Finally, the designed PIN (P3HT-blend-PCBM) structure was obtained by thermally depositing another PCBM layer (20 nm thick, regarded as N-layer) on top of the PI (P3HT-blend) layer. To complete the device fabrication, 50 nm-thick Al electrodes were thermally deposited on the PIN film via a shadow copper grid mask (See Method for more details), resulting in a channel width of 2000 μm and a channel length of 10 μm.

A conceptual schematic of the PIN photoconductor and the molecular structures of the used organic materials (P3HT and PCBM) are illustrated in Figure 1a. Figure 1b presents the cross-sectional scanning electron microscopy (SEM) of the PIN film. Different conductivity of organic layer shows different color in the SEM image. Here we believe the white color represents the PCBM layer, the dark color represents the P3HT layer and the gray color between the white and dark color should be I layer. The energy band diagrams of P3HT and PCBM are presented in Figure 1c, from which it can be clearly seen that the electrons will flow from P3HT into PCBM owing to the relative positions of their energy levels[23,24]. The surface evolution during the processes of PIN film formation is characterized by Atomic force microscopy (AFM) (shown in Figure 2). Known from the AFM graphs, the initial P3HT layer has very smooth surface (Figure 2a and 2e), after thermal deposition of PCBM onto the uniform P3HT film, small grains are formed (seen in Figure 2b, f). During the DCM solvent annealing process, the PCBM grains absorb the DCM vapor and diffuse into the underlying P3HT layer, forming the P3HT-blend layer (PI), such process produces a quite rough surface (seen in Figure 2c, g). Another deposited PCBM layer (N layer) fully covers the PI film and shows a similar roughness, which basically follows that of the underlying PI film (seen in Figure 2d, h).

We performed X-ray diffraction (XRD) measurements on the pristine PCBM film (40 nm, thermally deposited), the pristine P3HT film (~500 nm), the PIN film and a spin-coated P3HT: PCBM blend film (~500 nm, weight ratio of P3HT to PCBM is 1:1). The PCBM film does not show any XRD information, and
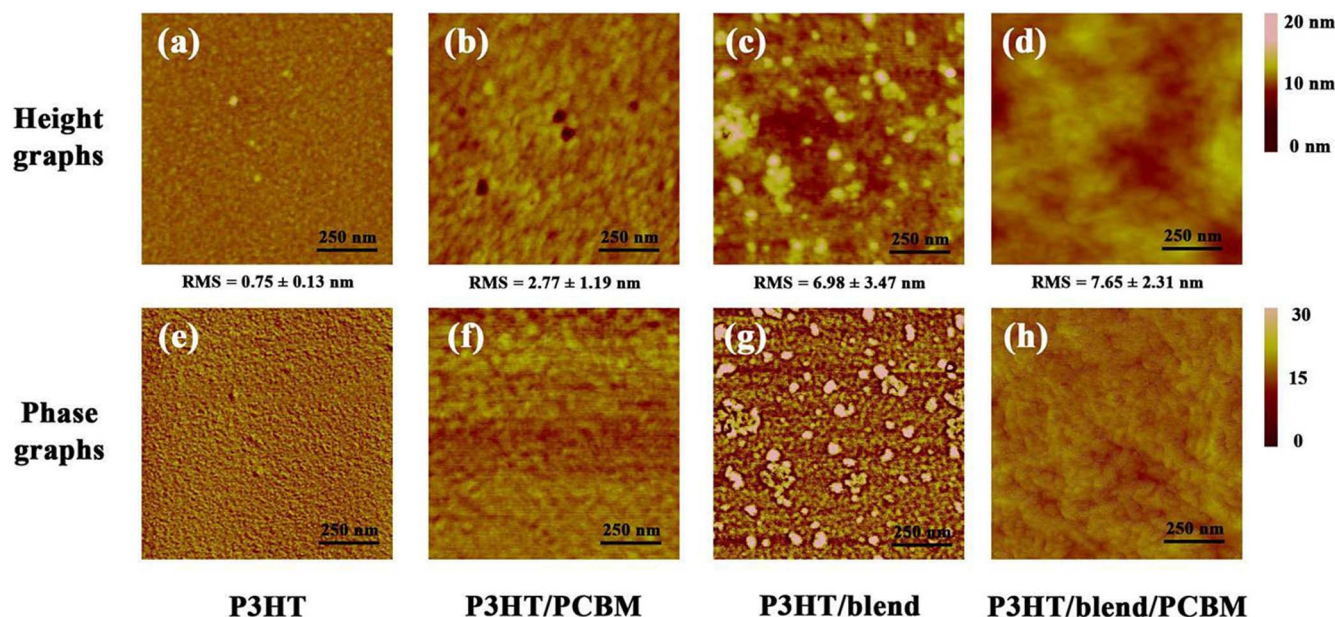

Figure 2 | **AFM images for the top view of the P3HT, P3HT/PCBM, P3HT/blend and P3HT/blend/PCBM.** (a), (b), (c), (d) for height and (e), (f), (g), (h) for phase.
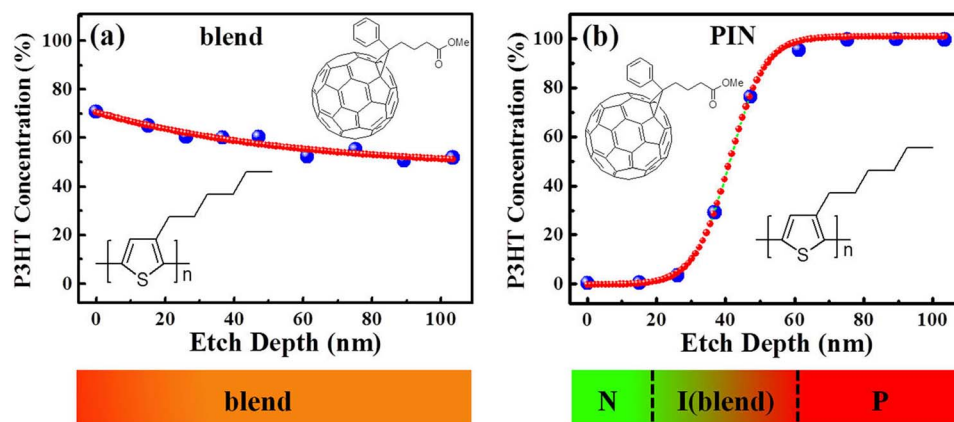
Figure 3 | Vertical composition profiles from surface (deduced via etching and XPS characterization): (a) for the blend film and (b) for the PIN film.

the rest three films all display two XRD peaks, which are from P3HT[25] (seen in Figure S2). We also analyzed the concentration-depth profile of the PIN film at the vertical direction (perpendicular to the surface) by using a well-established technique (slowly etching the prepared film from the surface accompanied with XPS measurement)[26]. The chemical composition of the pristine P3HT film and the pristine PCBM film were first analyzed via XPS in order to facilitate the calculation of the P3HT and PCBM composition in the PIN film along the vertical direction. Figure S3a provides detailed information about the XPS test on the P3HT film, where the S 2p peak (located at 163.17 eV) can be clearly seen, which is regarded as the character peak for P3HT. Figure S3b provides that of the PCBM film, in which the O 2p peak (located at 532.71 eV), the character peak for PCBM, is clearly shown. The XPS results on P3HT and PCBM are in well agreement with that reported by other research groups[27]. By measuring the intensity of O 1s and S 2p, the distribution of P3HT and PCBM along the vertical direction from the surface can be calculated[27]. The XPS results of the blend film and the PIN film are given in Figure S4a and Figure S4b, respectively. The calculated P3HT concentration-depth profiles of the two films are presented in Figure 3a and Figure 3b, respectively.

Seen in Figure 3a, the blend film gradually changes from P3HT-rich near the surface to PCBM-rich close to the substrate, consistent with the reported[27,28]. For the PIN film (shown in Figure 3b), the top ~20 nm from the surface is consisted of only PCBM (without P3HT), the concentration of P3HT then starts to increase from 0%, and reaches 100% when the depth from the surface reaches ~60 nm, and it remains unchanged with further increasing the depth (for this reason, we only etched 140 nm from the surface for the XPS measurement). The results give a strong evidence that our film is indeed PIN structure: P3HT (~500 nm)/P3HT:PCBM blend (~40 nm)/PCBM (~20 nm).

The UV-Vis absorption spectra and Photoluminescence (PL) spectra of the PCBM film, the P3HT film, the blend film and the PIN film are given in Figure 4. In the UV-Vis absorption spectra (Figure 4a), P3HT shows broad absorption in a range from 450 to 620 nm, while PCBM mainly absorbs light in the UV region (peaks at 347 nm). The PIN film and the blend film exhibit wide absorption covering that of both P3HT and PCBM. It is well-known that P3HT shows high PL intensity while PCBM is an extremely efficient PL quencher. When blending the polymer with the fullerene molecules, a strong reduction in the PL quantum yield is clearly seen. This phenomenon is induced by the efficient charge transfer between the polymer chains and fullerene molecules[29,30]. In Figure 4b it is apparent that the PL intensity for the PIN film is weaker than that of the P3HT film, which should be originated from the formation of the I layer.

For a photoconductor device, it is well known that the light response is closely related to the responsivity R (a parameter characterizing the sensitivity of the device to light) and photo gain G (a parameter characterizing the creation of an electron-hole pair on absorption of a photon results in an increase in conductivity that persists for the excited carrier lifetime). R is defined by the following equation[31,32]:

$$R = \frac{I_{Light} - I_{Dark}}{P_{ill}} = EQE\frac{\lambda q}{hc}G \approx (1-T)\frac{\lambda q}{hc}G \qquad (1)$$

Where I_{Light} is current under the illumination, I_{Dark} is the dark current, P_{ill} is the incident illumination power on the effective area (channel area), EQE is the external quantum efficiency, λ is the wavelength of interest, q is the electron charge, h is the Planck constant, c is the speed of light and T is the transmission of light through the film. G is defined as the ratio between the number of electrons collected per unit time and the number of absorbed photons per unit time, and can be expressed by the following equation[31,33]:

$$G = \frac{\left(\mu_n + \mu_p\right)\tau E}{L} \qquad (2)$$

Where μ_n is the electron mobility, μ_p is the hole mobility, τ is the photo carrier lifetime, E is the electrical field and L is the device channel length.

From the Equation (1) and (2), it is seen that both R and G are proportional to carrier mobility μ, we thereby fabricated field effect transistors (FETs) and extracted carrier mobilities in each films involved in this study (from their transfer curves shown in Figure S5), which are listed here: hole mobilities in the P3HT film and the blend film are 2.8×10^{-2} and 1.5×10^{-5} cm²V⁻¹s⁻¹, respectively. Electron mobilities in the PCBM film and the blend film are 3.1×10^{-3} and 1.8×10^{-4} cm²V⁻¹s⁻¹, respectively. These mobility values are consistent with the reported ones[34–36].

The performances of the fabricated photoconductors based on the PCBM film, the P3HT film, the blend film and the PIN film are compared under an incident light density of 10.6 μWcm⁻² at 600 nm. The PCBM film shows very poor photocurrent (seen in Figure S6), and this should be induced by its large band gap (2.4 eV), low electron mobility (3.1×10^{-3} cm²V⁻¹s⁻¹) and low conductivity[37,38]. The P3HT film has much higher photocurrent (seen in Figure 5a), which can be attributed to its small band gap (1.9 eV), high hole mobility (2.8×10^{-2} cm²V⁻¹s⁻¹) and high conductivity[37,38]. Because of the high exciton binding energy in conjugated polymers, thermal energy at room temperature is not sufficient to dissociate a photo exciton (typical with a binding energy of 0.4 eV) into free charge carriers[8]. The free carriers that form the photo-
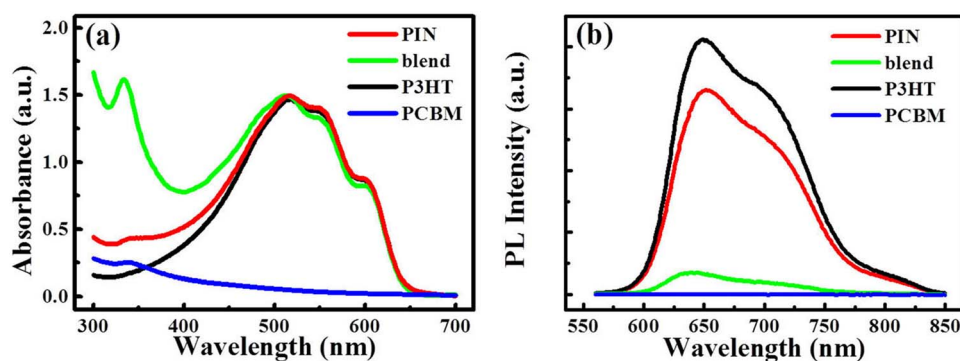
Figure 4 | (a) Absorption spectra and (b) PL spectra of the PCBM film, the P3HT film, the blend film and the PIN film.

current in the PCBM film and the P3HT film should come from photo exciton dissociation induced by the external electric field and impurity inside the film[39].The blend film shows much higher photocurrent in comparison to that of the P3HT film and the PCBM film (seen in Figure 5d). Considering that hole mobility in the blend film (1.5×10^{-5} cm²V⁻¹s⁻¹) is actually much lower than that in the P3HT film (2.8×10^{-2} cm²V⁻¹s⁻¹), and electron mobility in the blend layer (1.8×10^{-4} cm²V⁻¹s⁻¹) is also much lower than that in the PCBM film (3.1×10^{-3} cm²V⁻¹s⁻¹), the larger photocurrent of the blend film obviously is induced by the greatly strengthened photo exciton dissociation, which produces much more free car-

riers[8,9,40]. The PIN film exhibits significantly higher photocurrent than the blend film (seen in Figure 5g). This can be understood in the following way: photo excitons are firstly dissociated at the P3HT/ PCBM interface in I-layer, electrons then would diffuse from the PCBM in the I-layer into the PCBM N-layer (on top) and holes would diffuse from the P3HT in the I-layer into the P3HT P-layer (on bottom) because of the higher carrier concentrations in the I-layer, which is the main source of the device to generate free carriers. Electrons then are transported in the N-layer and holes are transported in the P-layer between the two electrodes under a bias. Since the N-layer has much higher electron mobility than that of the blend
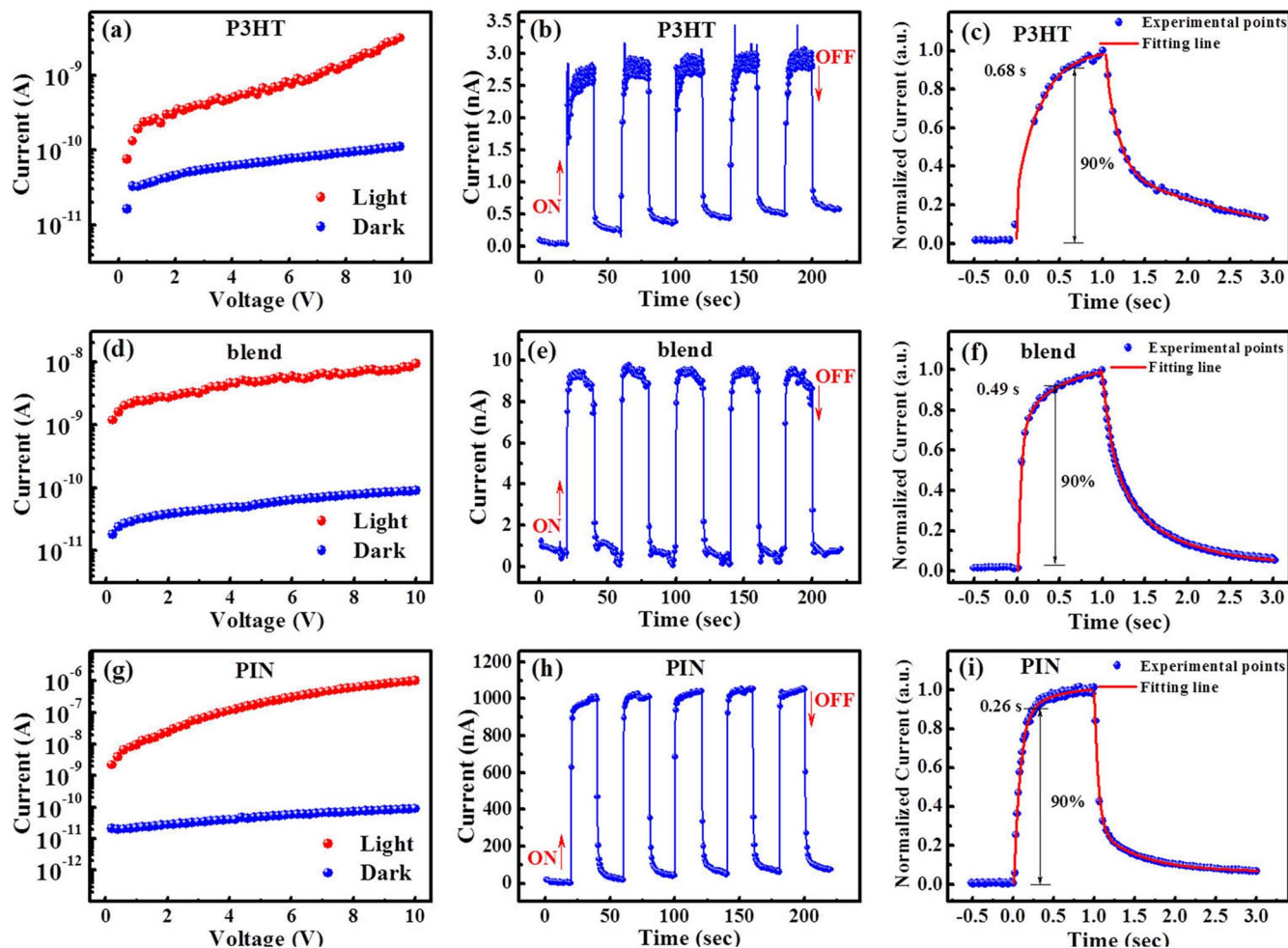

Figure 5 | I–V curves, On/Off switching properties (at a bias of 10 V) and time resolved photocurrent (at a bias of 10 V) of the investigated devices under an incident light density of 10.6 μWcm⁻² at 600 nm. (a, b, c) for the P3HT device, (d, e, f) for the blend device and (g, h, i) for the PIN device. Various parameters extracted from these figures are listed in Table 1.
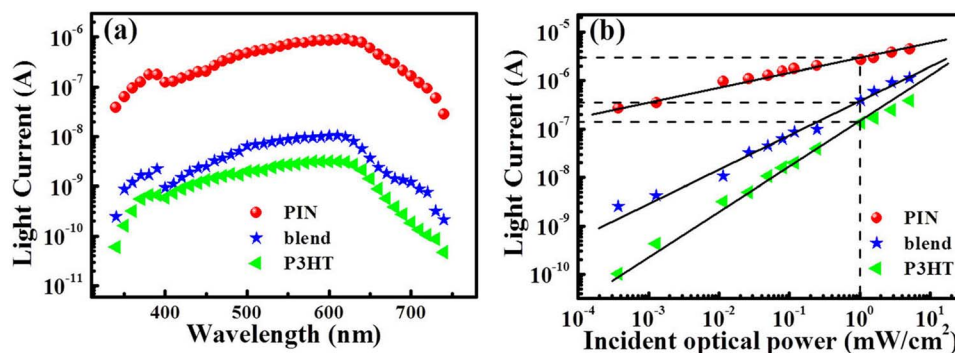
Figure 6 | Comparison of light current between the P3HT device, the blend device and the PIN device: (a) spectral based light current, (b) LDR measured under an incident light at 600 nm. All of the measurements were done at a bias of 10 V.

film (3.1×10^{-3} vs 1.8×10^{-4} cm²V⁻¹s⁻¹), and the P-layer has much higher hole mobility than that in the blend film (2.8×10^{-2} vs 1.5×10^{-5} cm²V⁻¹s⁻¹), the photocurrent is thereby greatly enhanced (in comparison to that of the blend film). It is worth noting here that holes in the P-layer should be collected by firstly transporting into the I-layer (40 nm, which is able to transport both electrons and holes), and then tunneling through the N-layer (20 nm). Also, in reality, the Al atoms could seep into the N-layer during thermal deposition, which plays a role of bring closer the I-layer and the electrode, and hence help holes transport through the N-layer. Similar charge transport can be found in literatures[41–43]. We also fabricated photoconductors with PN structure (P3HT/PCBM) and PI structure (P3HT/blend). For the PN structure, although the hole/electron mobility is high, the P (P3HT)/N (PCBM) interface is not sufficient enough to generate enough free carriers. For the PI structure, the electron mobility is low, limiting its photoresponse capability. Hence photoresponses of both the PN structure and the PI structure are weaker than the PIN structure (I–V curves shown in Figure S7).

Figure 5b, e and h present the on-off switching characteristics (at a bias of 10V) of photoconductors based on the P3HT film, the blend film and the PIN film, respectively. The ON and OFF time durations are both 20 seconds for all the three devices. It is clearly seen that all the devices can be switched on and off repeatedly. Figure 5c, f and i present the light rise/decay information (at a bias of 10 V) of the photoconductors based on the P3HT film, the blend film and the PIN film, respectively. The rise/decay dynamic response of these devices can be described by two exponential equations from the time-resolved photocurrent response, which are widely used in the area of photoconductors[44,45] (The mathematical equations can be found in the Supporting Information and Methods section). The light rise/decay experimental data can be well fitted by the two equations. For the P3HT device, the light rise time (switch-on) is 0.68 s and the decay time (switch-off) is 3.12 s. The photocurrent of the P3HT film mainly comes from photo-exciton dissociation induced by the external electric field and impurity inside the film[39]. Owing to the fact that carrier trapping/detrapping process needs a long time, thereby the light rise/decay times is quite large for the P3HT device[39]. For the blend device, the light rise/decay time is 0.49/1.01 s, smaller than that of the P3HT device due to the much faster free carrier generation and recombination processes: photo exciton is mainly dissociated and recombined via donor/acceptor interface in the blend film[46,47]. The PIN device exhibits shorter response/decay time of 0.26/0.84 s in comparison to that of the blend device, this can be attributed to the faster carrier transport process resulted from its much higher carrier mobilities.

Figure 6a shows light current as a function of wavelength for the P3HT device, the blend device and the PIN device (under a bias of 10 V and an incident light density of 10.6 µWcm⁻²). It is seen that across all the investigated wavelengths, photocurrent of the PIN device is several orders higher than that of the P3HT device and

the blend device, which further demonstrates the advantage of the PIN architecture.

Except for R and G, the other three figure of merits for evaluating a photoconductor device are the normalized detectivity (D*, in units of Jones to characterize the sensitivity), signal to noise ratio (SNR) and the linear dynamic range (LDR, typically quoted in dB to measure the linearity of the photocurrent versus incident optical power). The D* can be expressed as[44]:

$$D^* = R_\lambda \sqrt{\frac{S}{2qI_{Dark}}} \qquad (3)$$

Where S is the effective area under illumination. SNR is defined by the following equation[48]:

$$SNR = \frac{I_{Light} - I_{Dark}}{I_{Dark}} \qquad (4)$$

LDR is given by the following equation[49]:

$$LDR = 20\log\left(\frac{J_{Light}}{J_{Dark}}\right) \qquad (5)$$

Where J_{Light} is the photocurrent density with a light intensity of 1 mWcm⁻², J_{Dark} is the dark current density.

Based on Equation (1–4) and the experiment results shown in Figure 5, we calculated G, R, D* and SNR values of the P3HT device, the blend device and the PIN device as a function of voltage, and they are shown in Figure S8. It is seen that the PIN device displays much better performance than that of the P3HT device and the blend device. For example, at a bias of 10 V, the PIN device shows G, R, D* and SNR values (200, 96.5 AW⁻¹, 5.69×10^{14} Jones and 1.14×10^4, respectively) much higher than that of the P3HT device (0.56, 0.27 AW⁻¹, 1.43×10^{12} Jones and 27, respectively) and the blend device (1.81, 0.87 AW⁻¹, 5.11×10^{12} Jones and 101, respectively). Figure 6b shows the photocurrent vs incident light density at 600 nm for the three devices at a bias of 10 V, from which LDR can be calculated based on Equation (5). The calculated LDR of the PIN device is 90 dB (a value is typically required for most imaging applications[50]), which is largely improved compared with that of the P3HT device (62 dB) and the blend device (73 dB). All parameters for all the investigated devices in this paper under a bias of 10 V are listed in Table 1. These results clearly indicate that the PIN architecture has great advantages over that of the conventional blend-based organic photoconductors.

Discussion

In summary, a PIN architecture for ultrasensitive OTFPs is demonstrated. In the PIN photoconductor, free photo carriers are mainly generated in the I-layer (P3HT:PCBM), electrons in the I-layer then will diffuse into the N-layer (PCBM) and are then transported in the

Table 1 | Parameters of the investigated photoconductors extracted from Figure 5 and Figure 6

Figure of merits	T Rise [s]	T Decay [s]	G	R [AW⁻¹]	D* [Jones]	SNR	LDR [dB]
P3HT	0.68	3.12	0.56	0.27	1.43×10^{12}	27	62
blend	0.49	1.01	1.81	0.87	5.11×10^{12}	101	73
PIN	0.26	0.64	200	96.5	5.69×10^{14}	1.14×10^{4}	90

N-layer, while holes will diffuse into the P-layer (P3HT) and are then transported in the P-layer. Because the P-layer (N-layer) has much higher hole (electron) mobility than the conventional blend film, carrier transport is thereby greatly enhanced. The values of R, D*, G and LDR for the PIN photoconductor are 96.5 AW⁻¹, 5.69×10^{14} Jones, 200 and 90 dB, respectively, which are much higher than the conventional bare blend based device (0.87 AW⁻¹, 5.11×10^{12} Jones, 1.81, 72 dB, respectively). These values represent the best results for OTFPs reported so far. It is clear that the performance can be further promoted by using organic materials with better absorption abilities and higher carrier mobilities. The PIN structure we designed here and the principle it demonstrated could open a new way for high-performance OTFPs.

Method

Material Preparation. All of the materials were purchased from Sigma-Aldrich and were used as received without further purification. The Corning Eagle XG glasses and N-doped silicon with 300 nm silicon dioxide were used as the substrates.

Solution Ratio and Concentration. The concentration of the rr-P3HT solution and the blend solution (P3HT:PCBM ratio of 1 : 1) in o-dichlorobenzene were 40 mg/ml. The solution was stirred rigorously for ca. 24 h at 50°C.

Device Fabrication. The P3HT film (~500 nm) and the P3HT:PCBM blend film (~500 nm) were formed by spin-coating the solution onto the substrate at 500 rpm for 5 seconds and subsequently at 1000 rpm for 30 seconds. The spin coated films were then left in a covered glass petri dish to dry the solvent out of the organic active layer. The coated organic film was then soft-baked on a hot plate at 110°C for 10 min. The PCBM film was formed by thermal deposition (40 nm at a rate of 0.05 nm/s). For the PIN film, a 20 nm thick PCBM was first evaporated onto the prepared P3HT film (~500 nm) and then put into a vessel for 60 s together with DCM (to generate DCM vapor to dissolve PCBM and bring PCBM mixing into P3HT). After thermally depositing another 20 nm PCBM, the PIN (P3HT-blend-PCBM) film is obtained. Photoconductor devices (for the PIN film, the P3HT film, the PCBM film and the P3HT:PCBM blend film) were fabricated on glass substrates while thin film transistors (TFTs) (for the P3HT film, the PCBM film, and the P3HT:PCBM blend film) were fabricated directly on SiO₂ (300 nm)/Si⁺ substrate. After the films were prepared, the devices were completed with thermal evaporation of 50 nm-thick Aluminum electrodes through a shadow copper grid mask which results in a channel width of 2000 μm and a channel length of 10 μm (for testing the hole mobility in P3HT TFT, Gold electrodes instead of Aluminum electrodes were used).

Measurement. Electrical characterizations were recorded with a Keithley 4200 and a Micromanipulator 6150 probe station at room temperature. The monochromatic light (produced by the spectrophotometer with a halogen–tungsten lamp) is from a Newport Oriel 200™. Prior to the use of the light, the spectral response and the light intensity were calibrated using a mono-silicon detector produced by the National Renewable Energy Laboratory (NREL). The device cross-sectional image was characterized by SEM (Hitachi S-4800). The AFM images were acquired using a Veeco NanoScope IV with a silicon cantilever in tapping mode. The XPS measurements were performed in a Kratos Ultra Spectrometer (a base pressure of 1×10^{-9} Torr) using monochromatized Al Kα X-ray photons (hυ = 1486.6 eV) discharge lamp. UV-vis spectra were recorded using JASCO V-570 spectrophotometer and PL spectra were characterized using JASCO FP-6600 spectrophotometer with a Xenon flash lamp. The phase identification was determined by using a Rifaku D/MAX-2004 XRD with Cu Kα radiation (λ = 1.54178 Å) operating at 40 KV and 60 mA.

1. Dong, G., Hu, Y., Jiang, C., Wang, L. & Qiu, Y. Organic photocouplers consisting of organic light-emitting diodes and organic photoresistors. *Appl. Phys. Lett.* **88**, 051110-051110-051113 (2006).
2. Sun, Q., Dong, G., Wang, L. & Qiu, Y. Organic optocouplers. *Sci. China Chem.* **54**, 1017–1026 (2011).
3. Martino, N., Ghezzi, D., Benfenati, F., Lanzani, G. & Antognazza, M. R. Organic semiconductors for artificial vision. *J. Mater. Chem. B* **1**, 3768–3780 (2013).
4. Baeg, K. J., Binda, M., Natali, D., Caironi, M. & Noh, Y. Y. Organic Light Detectors: Photodiodes and Phototransistors. *Adv. Mater.* **25**, 4267–4295 (2013).

5. Iacchetti, A., Natali, D., Binda, M., Beverina, L. & Sampietro, M. Hopping photoconductivity in an exponential density of states. *Appl. Phys. Lett.* **101**, 103307-103307-103304 (2012).
6. Jin, Z., Gao, L., Zhou, Q. & Wang, J. High-performance flexible ultraviolet photoconductors based on solution-processed ultrathin ZnO/Au nanoparticle composite films. *Sci. Rep.* **4**, 4268 (2014).
7. Günes, S., Neugebauer, H. & Sariciftci, N. S. Conjugated polymer-based organic solar cells. *Chem. Rev.* **107**, 1324–1338 (2007).
8. Blom, P. W., Mihailetchi, V. D., Koster, L. J. A. & Markov, D. E. Device physics of polymer: fullerene bulk heterojunction solar cells. *Adv. Mater.* **19**, 1551–1566 (2007).
9. Yu, G., Gao, J., Hummelen, J., Wudl, F. & Heeger, A. Polymer photovoltaic cells: enhanced efficiencies via a network of internal donor-acceptor heterojunctions. *Science* **270**, 1789–1790 (1995).
10. Dang, M. T., Hirsch, L. & Wantz, G. P3HT: PCBM, best seller in polymer photovoltaic research. *Adv. Mater.* **23**, 3597–3602 (2011).
11. Erb, T. *et al.* Correlation between structural and optical properties of composite polymer/fullerene films for organic solar cells. *Adv. Funct. Mater.* **15**, 1193–1196 (2005).
12. Jeong, J. W. *et al.* Interdigitated electrode geometry effects on the performance of organic photoconductors for optical sensor applications. *Thin Solid Films* **518**, 6343–6347 (2010).
13. Peet, J. *et al.* Method for increasing the photoconductive response in conjugated polymer/fullerene composites. *Appl. Phys. Lett.* **89**, 252105 (2006).
14. Jin, Z., Liu, G. & Wang, J. Organic nonvolatile resistive memory devices based on thermally deposited Au nanoparticle. *AIP Adv.* **3**, 052113 (2013).
15. Li, S.-M. *et al.* Improving the Photo Current of the [60]PCBM/P3HT Photodetector Device by using Wavelength-matched Photonic Crystals. *J. Mater. Chem.C.* **2**, 1500–1504 (2014).
16. Wienk, M. M. *et al.* Efficient methano [70]fullerene/MDMO-PPV bulk heterojunction photovoltaic cells. *Angew. Chem.* **115**, 3493–3497 (2003).
17. Von Hauff, E., Dyakonov, V. & Parisi, J. Study of field effect mobility in PCBM films and P3HT: PCBM blends. *Sol. Energy Mater. Sol. Cells* **87**, 149–156 (2005).
18. Granström, M. *et al.* Laminated fabrication of polymeric photovoltaic diodes. *Nature* **395**, 257–260 (1998).
19. Siebert-Henze, E. *et al.* Electroabsorption studies of organic pin solar cells: Increase of the built-in voltage by higher doping concentration in the hole transport layer. *Org. Electron.* **15**, 563–568 (2014).
20. Li, G. *et al.* "Solvent Annealing" Effect in Polymer Solar Cells Based on Poly(3-hexylthiophene) and Methanofullerenes. *Adv. Funct. Mater.* **17**, 1636–1644 (2007).
21. Dennler, G. *et al.* Enhanced spectral coverage in tandem organic solar cells. *Appl. Phys. Lett.* **89**, 073502-073502-073503 (2006).
22. Ayzner, A. L., Tassone, C. J., Tolbert, S. H. & Schwartz, B. J. Reappraising the need for bulk heterojunctions in polymer-fullerene photovoltaics: the role of carrier transport in all-solution-processed P3HT/PCBM bilayer solar cells. *J.Phys.Chem.C.* **113**, 20050–20060 (2009).
23. Kim, J. Y. *et al.* New Architecture for High-Efficiency Polymer Photovoltaic Cells Using Solution-Based Titanium Oxide as an Optical Spacer. *Adv. Mater.* **18**, 572–576 (2006).
24. Kim, J. Y. *et al.* Efficient Tandem Polymer Solar Cells Fabricated by All-Solution Processing. *Science* **317**, 222–225 (2007).
25. Nguyen, L. H. *et al.* Effects of Annealing on the Nanomorphology and Performance of Poly(alkylthiophene):Fullerene Bulk-Heterojunction Solar Cells. *Adv. Funct. Mater.* **17**, 1071–1078 (2007).
26. Hori, T. *et al.* Active layer analysis of interpenetrating heterojunction organic thin-film solar cells by X-ray photoelectron spectroscopy. *Thin Solid Films* **554**, 222–225 (2014).
27. Guan, Z.-L. *et al.* Direct determination of the electronic structure of the poly (3-hexylthiophene): phenyl-[6,6]-C61 butyric acid methyl ester blend. *Org. Electron.* **11**, 1779–1785 (2010).
28. Campoy-Quiles, M. *et al.* Morphology evolution via self-organization and lateral and vertical diffusion in polymer:fullerene solar cell blends. *Nat. Mater.* **7**, 158–164 (2008).
29. Campoy-Quiles, M., Kanai, Y., El-Basaty, A., Sakai, H. & Murata, H. Ternary mixing: A simple method to tailor the morphology of organic solar cells. *Org. Electron.* **10**, 1120–1132 (2009).
30. van Bavel, S. S., Bärenklau, M., de With, G., Hoppe, H. & Loos, J. P3HT/PCBM Bulk Heterojunction Solar Cells: Impact of Blend Composition and 3D Morphology on Device Performance. *Adv. Funct. Mater.* **20**, 1458–1463 (2010).
31. Jin, Z. & Wang, J. Flexible high-performance ultraviolet photoconductor with zinc oxide nanorods and 8-hydroxyquinoline. *J. Mater. Chem.C.* **2**, 1966–1970 (2014).

32. Zhou, Y., Wang, L., Wang, J., Pei, J. & Cao, Y. Highly Sensitive, Air-Stable Photodetectors Based on Single Organic Sub-micrometer Ribbons Self-Assembled through Solution Processing. *Adv. Mater.* **20**, 3745–3749 (2008).

33. Jin, Z. & Wang, J. High-responsivity solution-processed organic-inorganic hybrid bilayer thin film photoconductors. *J. Mater. Chem.C.* **1**, 7996–8002 (2013).

34. Hamilton, M. C., Martin, S. & Kanicki, J. Thin-film organic polymer phototransistors. *IEEE T. Electron Dev.* **51**, 877–885 (2004).

35. Bao, Z., Dodabalapur, A. & Lovinger, A. J. Soluble and processable regioregular poly(3-hexylthiophene) for thin film field-effect transistor applications with high mobility. *Appl. Phys. Lett.* **69**, 4108 (1996).

36. Chang, J.-F. *et al.* Enhanced mobility of poly (3-hexylthiophene) transistors by spin-coating from high-boiling-point solvents. *Chem. Mater.* **16**, 4772–4776 (2004).

37. Schafferhans, J., Baumann, A., Wagenpfahl, A., Deibel, C. & Dyakonov, V. Oxygen doping of P3HT: PCBM blends: Influence on trap states, charge carrier mobility and solar cell performance. *Org. Electron.* **11**, 1693–1700 (2010).

38. Glatthaar, M. *et al.* Efficiency limiting factors of organic bulk heterojunction solar cells identified by electrical impedance spectroscopy. *Sol. Energy Mater. Sol. Cells* **91**, 390–393 (2007).

39. Yang, K., Wang, Y., Jain, A., Samulson, L. & Kumar, J. Determination of Electron and Hole Mobility of Regioregular Poly(3-hexylthiophene) by the Time of Flight Method. *J. Macromol. Sci. Part A-Pure Appl. Chem.* **44**, 1261–1264 (2007).

40. Marsh, R. A., Hodgkiss, J. M., Albert-Seifried, S. & Friend, R. H. Effect of Annealing on P3HT:PCBM Charge Transfer and Nanoscale Morphology Probed by Ultrafast Spectroscopy. *Nano Lett.* **10**, 923–930 (2010).

41. Capelli, R. *et al.* Organic light-emitting transistors with an efficiency that outperforms the equivalent light-emitting diodes. *Nat. Mater.* **9**, 496–503 (2010).

42. Wang, H. *et al.* Ambipolar organic field-effect transistors with air stability, high mobility, and balanced transport. *Appl. Phys. Lett.* **88**, 133508-133508-133503 (2006).

43. Shi, J. *et al.* n-Channel, Ambipolar, and p-Channel Organic Heterojunction Transistors Fabricated with Various Film Morphologies. *Adv. Funct. Mater.* **17**, 397–400 (2007).

44. Jana, M. K. *et al.* Near infrared detectors based on HgSe and HgCdSe quantum dots generated at the liquid-liquid interface. *J. Mater. Chem.C.* **1**, 6184–6187 (2013).

45. Sun, Z. *et al.* Infrared Photodetectors Based on CVD-Grown Graphene and PbS Quantum Dots with Ultrahigh Responsivity. *Adv. Mater.* **24**, 5878–5883 (2012).

46. Chen, S. *et al.* Photo-Carrier Recombination in Polymer Solar Cells Based on P3HT and Silole-Based Copolymer. *Adv. Energy Mater.* **1**, 963–969 (2011).

47. Ferguson, A. J., Kopidakis, N., Shaheen, S. E. & Rumbles, G. Dark Carriers, Trapping, and Activation Control of Carrier Recombination in Neat P3HT and P3HT:PCBM Blends. *J.Phys.Chem.C.* **115**, 23134–23148 (2011).

48. Jin, Z. & Wang, J. A trilayer architecture for polymer photoconductors. *Appl. Phys. Lett.* **102**, 053304 (2013).

49. Gong, X. *et al.* High-Detectivity Polymer Photodetectors with Spectral Response from 300 nm to 1450 nm. *Science* **325**, 1665–1667 (2009).

50. Konstantatos, G., Clifford, J., Levina, L. & Sargent, E. H. Sensitive solution-processed visible-wavelength photodetectors. *Nat. Photonics* **1**, 531–534 (2007).

Author contributions

Z.J. performed the experimental work, the data analysis and the experimental planning; The project was conceived, planned and supervised by Z.J. and J.W.; The manuscript was written and reviewed by Z.J. and J.W.

Additional information